IOPscience iopscience.iop.org

Home Search Collections Journals About Contact us My IOPscience

Dielectric properties of the charge-ordered mixed oxide $CaMn_7O_{12}$

This article has been downloaded from IOPscience. Please scroll down to see the full text article.

2006 J. Phys.: Condens. Matter 18 3803

(http://iopscience.iop.org/0953-8984/18/15/023)

View the table of contents for this issue, or go to the journal homepage for more

Download details:
IP Address: 129.252.86.83
The article was downloaded on 28/05/2010 at 10:05

Please note that terms and conditions apply.

INSTITUTE OF PHYSICS PUBLISHING JOURNAL OF PHYSICS: CONDENSED MATTER

J. Phys.: Condens. Matter **18** (2006) 3803–3815 doi:10.1088/0953-8984/18/15/023

Dielectric properties of the charge-ordered mixed oxide $CaMn_7O_{12}$

A Castro-Couceiro[1], S Yáñez-Vilar[1], B Rivas-Murias[2], A Fondado[2], J Mira[2], J Rivas[2] and M A Señarís-Rodríguez[1]

[1] Departamento de Química Fundamental, Universidad de A Coruña, 15071 A Coruña, Spain
[2] Departamento de Física Aplicada, Universidad de Santiago, 15782 Santiago de Compostela, Spain

E-mail: tonasr@udc.es (M A Señarís-Rodríguez)

Received 24 October 2005, in final form 8 March 2006
Published 30 March 2006
Online at stacks.iop.org/JPhysCM/18/3803

Abstract

We present in this paper a detailed investigation of the dielectric properties of the mixed oxide $CaMn_7O_{12}$ that shows a charge-ordering transition at $T_{CO} = 440$ K. Surprisingly, this compound presents a high dielectric constant at room temperature. Data taken at several frequencies and temperatures point to relaxor dielectric behaviour, that can be attributed to the electronic inhomogeneities present in the material. Extrinsic Maxwell–Wagner effects make a significant contribution to this dielectric response, as revealed by the studies made on samples of different particle size and using different types of contact. The intrinsic dielectric constant of this material is $\varepsilon'_{r(intrinsic)} \sim 30$ at room temperature, a value that is relatively high for this type of compound and that we relate to the presence of the electronic process of charge ordering in this material.

1. Introduction

The search for materials with a high dielectric constant has long been a field of interest, due to the important applications of such a property in many electric and electronic devices, such as capacitors. Nowadays, the best industrial performances are given by ferroelectrics [1], i.e., substances with permanent electrical dipoles, even in the absence of an external electric field. In these materials the ferroelectric state arises because the centre of the positive charges in the lattice is displaced with respect to that of the negative charges. This is, its ultimate origin is structural. Among these ferroelectric substances are the well-known perovskite materials $BaTiO_3$, $PbTiO_3$, etc, that are the most widely used [1].

The possible existence of alternative dielectric materials with optimal dielectric properties is an attractive topic, especially after the recent discovery of a room-temperature frequency-independent 'colossal' dielectric constant in the complex mixed oxide $CaCu_3Ti_4O_{12}$ [2] whose

intrinsic or extrinsic origin has been intensively debated [3–6]. Particularly interesting and controversial is the possibility of obtaining very high (giant or even colossal) dielectric constants in which that property is based on purely electronic mechanisms. In this context, the existence of such a behaviour is normally associated to: (a) the presence of charge-density waves (CDWs), such as in the case of the blue bronze $K_{0.3}MoO_3$ in which a very high dielectric constant has been found [7] and explained on the basis of such an electronic feature [8]; (b) the proximity of a metal–insulator transition, as diverging dielectric constants are predicted for such a situation [9]; (c) highly correlated electron systems, with a strong Coulomb interaction between localized and itinerant electrons [10].

Looking for systems that could be good candidates to display high dielectric constants, we focused on mixed oxides that experience charge ordering (CO), i.e., mixed valent compounds in which the metal ions in different oxidation states order in specific lattice sites giving rise to charge localization. Materials with such transitions are not new [11], but they have recently received a lot of renewed attention in connection with the colossal magnetoresistance exhibited by some rare earth manganate series, some of them with CO [12].

In this paper we will describe the dielectric behaviour of one of these compounds: the manganese mixed oxide $CaMn_7O_{12}$ ($T_{CO} = 440$ K).

From the structural point of view, the compound $CaMn_7O_{12}$ belongs to the $(AA'_3)B_4O_{12}$ family, as can be more readily seen when formally writing its formula as $(CaMn_3^{3+})(Mn_3^{3+}Mn^{4+})O_{12}$. This perovskite-derived phase consists of a three-dimensional array of corner-sharing $[BO_6]$ octahedra that are tilted, so that one-quarter of the A-sites are distorted into icosahedra (that are occupied by Ca^{2+} ions) and three-quarters into tetracapped rhombic prisms that accommodate the Jahn–Teller Mn^{3+} ions.

Above 440 K, the formally Mn^{3+} and Mn^{4+} ions occupy at random the octahedral B-sites and the crystal symmetry is cubic ($Im\bar{3}$) [13] (figure 1). Nevertheless, at 440 K this compound experiences a structural phase transition associated to the electronic processes of charge ordering (CO) and orbital ordering (OO) [13]. Below 409 K, the crystal structure has trigonal symmetry (space group: $R\bar{3}$) [14], due to the ordering of the distinguishable Mn^{3+} and Mn^{4+} ions of the B sublattice into (9d) and (3b) sites [14]. These two phases coexist over the temperature interval 409 K $< T <$ 440 K.

From the magnetic point of view, this compound is paramagnetic above 86 K. Below 86 K, long-range magnetic ordering of the magnetic moments of Mn^{3+} and Mn^{4+} ions has been observed, and between 86 and 50 K two different ordered magnetic phases have been detected: one ferrimagnetic and another modulated [15].

We present in this paper a detailed study of the dielectric properties of $CaMn_7O_{12}$ as a function of temperature and frequency. In addition, in order to test the role of intrinsic and extrinsic factors on the observed dielectric properties we analyse the influence of factors such as the particle size of the polycrystalline samples and the electrode contacts.

2. Experimental details

To prepare $CaMn_7O_{12}$ polycrystalline materials with different particle size we have synthesized the samples by a soft-chemistry route: the so-called 'liquid-mix' or Pechini method [16], heating the precursor powders at different temperatures whose upper limit (T_{max}: 975 °C) was conditioned by the melting temperature of the compound. $CaCO_3$ (Panreac, >98.6%) and $Mn(NO_3)_2{\cdot}H_2O$ (Aldrich, >98%) were used as starting materials. The procedure was as follows. We dissolved stoichiometric amounts of these metallic salts in a 1 M citric acid aqueous solution. We then added the same volume of ethylene glycol, and we finally diluted the so-obtained solution in water (50% v/v). The resulting solution was heated at 200 °C until a

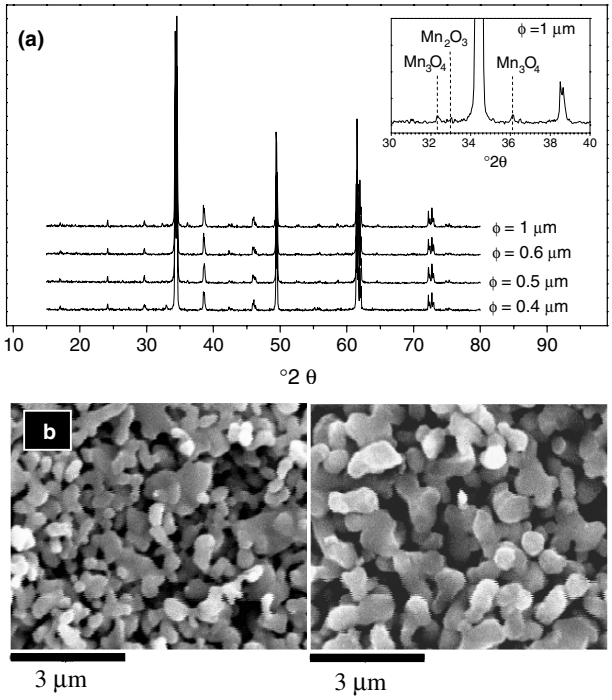

Figure 1. (a) Powder x-ray diffraction patterns for the different $CaMn_7O_{12}$ samples. Inset: enlargement of the Mn_2O_3 and Mn_3O_4 peaks detected in the samples with smallest and highest particle size diameter (ϕ). (b) SEM micrographs of the $CaMn_7O_{12}$ samples. Left: $\phi \sim 0.4$ μm ($T_{ann} = 925\,^{\circ}C$), right: $\phi \sim 1$ μm ($T_{ann} = 975\,^{\circ}C$).

Table 1. Accumulative thermal treatments given to the different samples after the initial common treatment at 800 °C, particle size of the so-obtained polycrystalline materials and total amount of secondary phases obtained from XRD Rietveld refinements.

Sample	Thermal treatments	Particle size ϕ (μm)	Total amount of secondary phases (%)
S1	925 °C/24 + 24 h	0.4	∼1.4
S2	925 °C/24 + 24 h + 950 °C/24 + 24 h	0.5	∼1.6
S3	900 °C/26 + 26 h + 950 °C/24 + 24 + 24 h	0.6	0
S4	925 °C/24 + 24 h + 950 °C/24 + 24 h + 975 °C/24 + 24 h	1	∼2.5

brown resin formed, whose organic matter subsequently decomposed at 400 °C. The precursor powders were first treated at 800 °C/48 h, and then pelletized and divided into four groups (S-1, S-2, S-3 and S-4). Each of these samples was then given different accumulative heating treatments at increasingly higher temperatures, as indicated in table 1.

Room-temperature x-ray powder diffraction (XRD) patterns of all the samples were obtained with a Siemens D-5000 diffractometer and Cu(Kα) = 1.5418 Å radiation. The obtained XRD data were analysed by the Rietveld profile analysis using the Rietica software [17].

The morphology and sizes of the particles were studied in a scanning electron microscope (SEM), JEOL 6400.

Their complex dielectric permittivity was measured with a parallel-plate capacitor coupled to a precision LCR meter Agilent 4284 A, capable of measuring in frequencies ranging from 20 to 10^6 Hz. The capacitor was mounted in an aluminium box refrigerated with liquid nitrogen, incorporating a mechanism to control the temperature up to 350 K. The samples in form of pellets with average diameter of 2 cm were prepared to fit in the capacitor, and gold was sputtered on their surfaces to ensure good electrical contact with the plates of the capacitor. Being aware of the controversy regarding extrinsic polarization effects as the origin of very high dielectric constants in other ceramic materials [3–6, 18, 19], additional measurements were performed using both silver paint and sputtered silver contacts.

Also, to test the optimal performance of the experimental set-up, a commercial $SrTiO_3$ sample was measured, and values similar to those reported in the literature [20] were obtained.

Complex plane analysis of the obtained impedance data was performed using the computer program LEVM [21].

3. Results

3.1. Sample characterization

According to the x-ray diffraction results, $CaMn_7O_{12}$ is the major phase in all the samples (figure 1(a)). Nevertheless, it is very difficult to obtain this compound as a completely single-phase material: in general, the presence of weak extra peaks in the XRD patterns (inset figure 1(a)) reveal the presence of small amounts of Mn_2O_3 and Mn_3O_4, that are difficult to eliminate completely, as also observed by other authors [22]. In any case, quantitative analysis of our XRD data by the Rietveld method indicates that these impurities, when present, represent in all cases minor amounts (table 1).

As for the cell parameters of the $CaMn_7O_{12}$ phase, the refinements give $a_h = 10.458$ Å and $c_h = 6.342$ Å, in good agreement with the data reported in the literature [15].

Morphologically, these polycrystalline materials consist of homogeneous, pseudo-spherical particles as seen in the corresponding SEM micrographs (figure 1(b)). Also, and as expected, the samples that have been annealed at lower temperatures and for shorter time show smaller particle size. In this context the averaged diameter (ϕ) of the particles changed from 1 μm in the sample annealed at a maximum temperature of 975 °C for 48 h to 0.4 μm in the sample annealed at a maximum temperature of 925 °C for 48 h (see figure 1(b) and table 1).

3.2. Dielectric properties

The relative complex dielectric permittivity of the samples, $\varepsilon_r = \varepsilon'_r - i\varepsilon''_r$ ($\varepsilon_r = \varepsilon/\varepsilon_0$, where $\varepsilon_0 = 8.85 \times 10^{-12}$ F m^{-1} is the permittivity of free space), as well as their ac conductivity, was measured as a function of frequency and temperature.

In what follows we will first describe the results obtained for the sample of higher particle size $\phi = 1$ μm (section 3.2.1) to then show the influence of particle size (section 3.2.2) and the type of contacts (section 3.2.3) on the measured dielectric properties.

3.2.1. Sample with $\phi = 1$ μm. Figure 2(a) shows the real part of the dielectric permittivity ε'_r (dielectric constant) as a function of temperature, obtained at different frequencies.

The first remarkable feature is the significant increase of this dielectric constant above a certain temperature, giving rise to a very high (giant) dielectric constant at room temperature ($10^4 < \varepsilon'_r \leqslant 10^6$). The temperature at which this increase takes place markedly shifts to higher values as the measuring frequency increases.

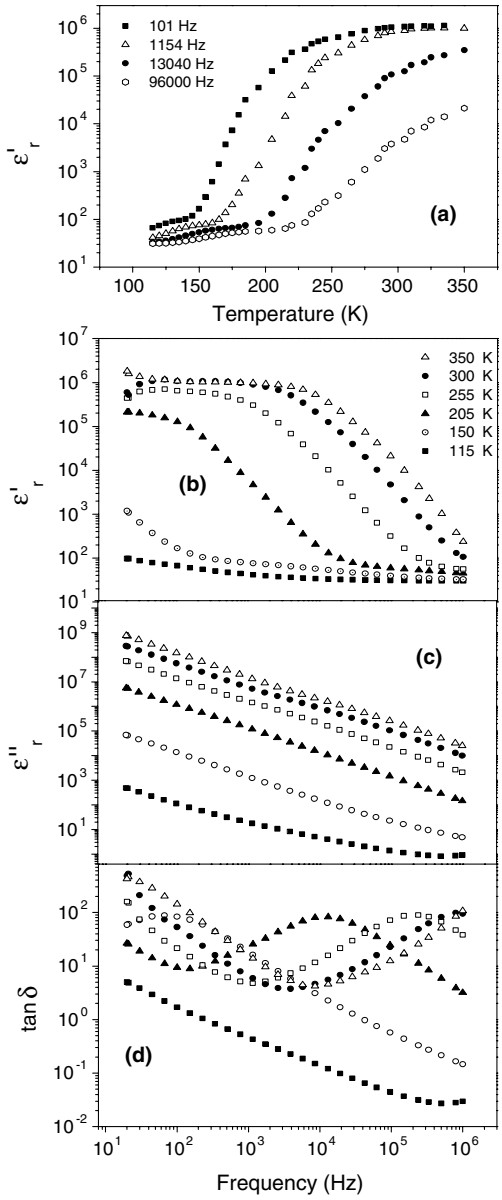

Figure 2. Dielectric behaviour of the sample with $\phi = 1\ \mu$m. (a) Temperature dependence of the real part of the dielectric permittivity (ε'_r) measured at four different frequencies ($101 \leqslant \nu(\text{Hz}) \leqslant 96\,000$). Frequency dependence of (b) the dielectric constant, (c) the imaginary part of the dielectric permittivity, and (d) the loss tangent measured at six different temperatures ($115\ \text{K} \leqslant T \leqslant 350\ \text{K}$).

The behaviour of the dielectric constant as a function of frequency is shown in figure 2(b). As can be seen, after a general initial decrease at very low frequencies, the giant dielectric constant maintains a constant value for a certain frequency range, giving rise to a 'plateau', and then decreases as frequency gets higher. It is also interesting that this plateau extends over larger frequency ranges as the temperature gets higher, so for $T = 350$ K these very high ε'_r values ($\varepsilon'_r \sim 10^6$) are retained up to 10^4 Hz.

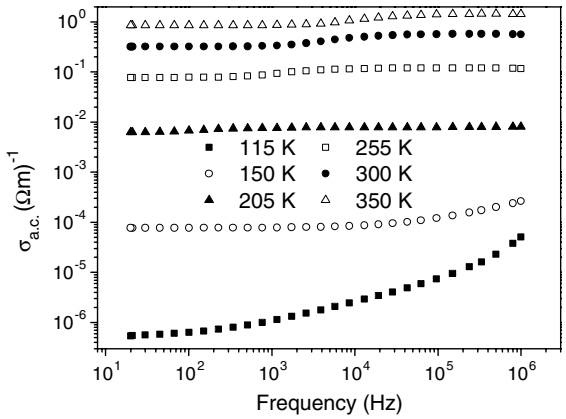

Figure 3. Conductivity versus frequency of the $CaMn_7O_{12}$ sample with $\phi \sim 1\ \mu$m. Temperature range: 115 K $\leqslant T \leqslant$ 350 K.

On the other hand, the imaginary part of the dielectric permittivity ε_r'' shows rather high values, that increase as the temperature rises and as frequency decreases (figure 2(c)). As a result, this sample shows rather high losses, as can be seen in figure 2(d), that shows the frequency dependence of the loss tangent, $\tan\delta = \varepsilon''/\varepsilon'$, at different temperatures.

The total conductivity of this $CaMn_7O_{12}$ sample, obtained from ac conductivity measurements (σ_{ac}), is shown in figure 3. As can be seen, this sample is not completely insulating and its conductivity increases with temperature. In addition, for $T \geqslant 300$ K the low-frequency σ_{ac} constant value experiences a sudden increase at $\nu \approx 10^4$ Hz, that is in fact the frequency at which the dielectric constant shows a step-like decrease.

3.2.2. Influence of the particle size. If we now compare the dielectric behaviour of the samples with different particle size as a function of temperature and as a function of frequency, we find the results that are summarized in figures 4(a)–(c). As can be observed, upon reduction of the particle size of these polycrystalline materials, the ε_r' values decrease by various orders of magnitude (figures 4(a) and (b)) and the extension of the plateau in the frequency domain slightly increases. In any case, at low temperatures and high frequencies the ε_r' of these samples converge in all cases to a similar value of the order of 30.

Another interesting aspect is the frequency dependence of the loss tangent of these samples (figure 4(c)). As can be seen, the dielectric losses increase further upon reduction of the particle size of these polycrystalline materials.

On the other hand, if for a given temperature we call ε_s' the value of the dielectric constant in the 'plateau' (where ε_r' remains constant), ε_∞' the ε_r' value obtained at the highest available frequency, $\Delta\varepsilon_r' = \varepsilon_s' - \varepsilon_\infty'$, and we plot $\Delta\varepsilon_r'$ on a semilogarithmic scale as a function of $1/\phi$, we find the results shown in figure 5. As can be observed, $\Delta\varepsilon_r'$ decreases linearly as the inverse of the particle diameter increases, that is, as the surface/volume ratio gets bigger.

In view of this linear dependence an extrapolation of $1/\phi$ towards zero gives $\Delta\varepsilon_r'$ ($\phi \to \infty$): 4.1×10^7 ($T = 300$ K), 3.4×10^7 ($T = 250$ K), and 1.5×10^7 ($T = 200$ K), for the case of an infinite grain size.

As for the conductivity of these samples, as expected, it is seen to decrease as the particle size decreases.

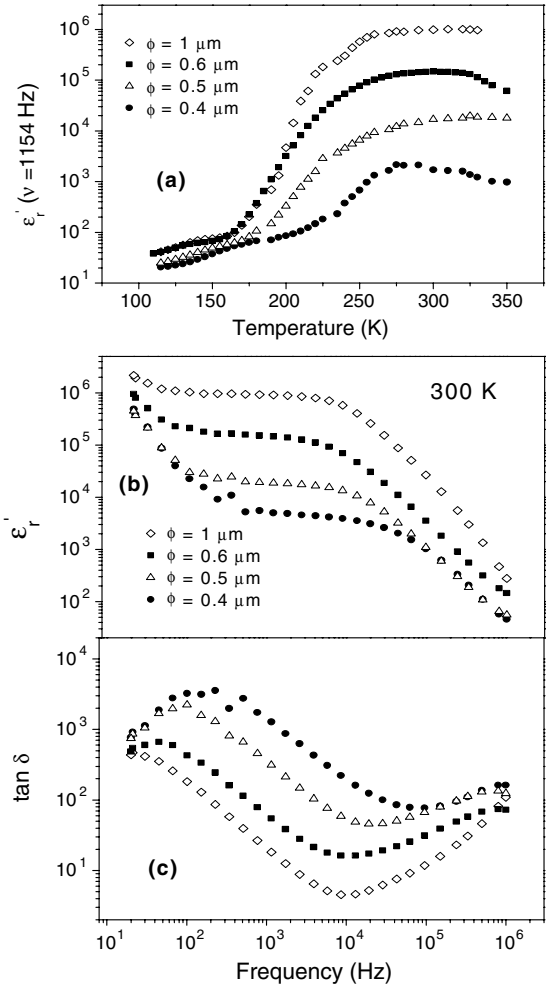

Figure 4. Comparison of the dielectric behaviour of $CaMn_7O_{12}$ samples with different particle size. (a) Temperature dependence of the dielectric constant (ε'_r) measured at 1154 Hz. (b) Frequency dependence of the imaginary dielectric constant at measured $T = 300$ K. (c) Frequency dependence of the loss tangent ($\tan\delta$) at $T = 305$ K.

3.2.3. Influence of the electrode contacts on the observed dielectric constant. We have measured the dielectric constant of these samples using different types of contact. As an example we show in figure 6(a) the results obtained on the sample with $\phi = 0.6$ μm using either sputtered gold or sputtered silver contacts. These measurements show that at low and medium frequency the type of electrode contact can cause a strong variation of ε'_r, and that the highest ε'_r values are obtained when using sputtered gold contacts. Nevertheless, at high frequencies ε'_r converges to similar values independently of the electrode contact used.

It is also worth pointing out that the samples with sputtered gold contacts are also those that show higher conductivity (figure 6(b)), and these differences remain to the highest frequencies.

4. Discussion

The dielectric behaviour reported here of the mixed oxide $CaMn_7O_{12}$ is very interesting from both the scientific and the technological points of view. In this context, the high dielectric

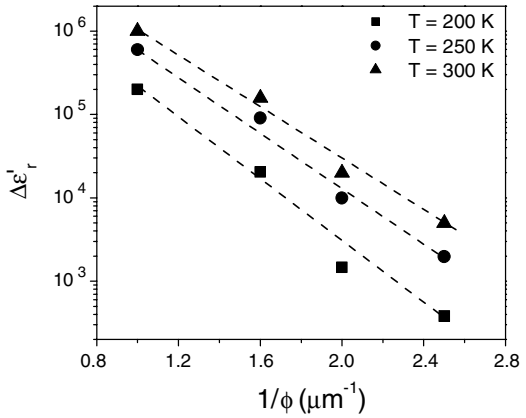

Figure 5. Plot of $\Delta\varepsilon'_r$ (on a semilogarithmic scale) versus the inverse of the particle size (ϕ) corresponding to the data obtained at three different temperatures, and corresponding linear fit (indicated by the dashed lines).

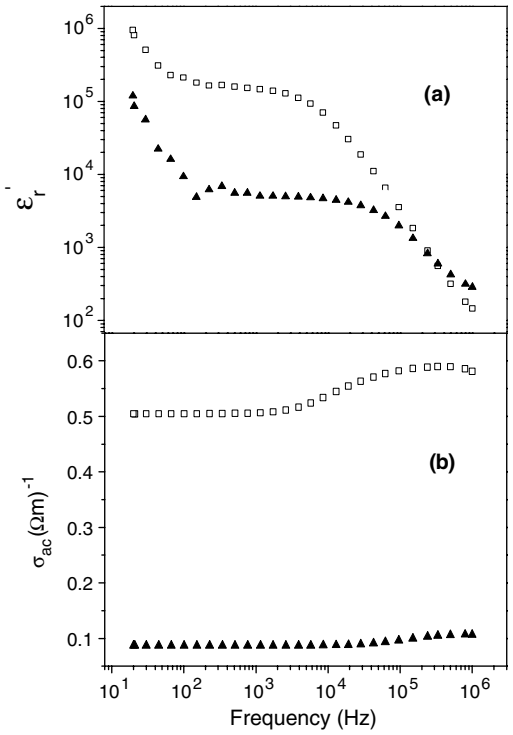

Figure 6. Influence of the type of contact (□ sputtered gold and ▲ sputtered silver) on the dielectric and electrical behaviour of the $CaMn_7O_{12}$ sample with $\phi = 0.6$ μm at $T = 300$ K. (a) Plot of ε'_r as function of frequency. (b) Plot of conductivity as a function of frequency.

constant of this compound at room temperature for frequencies up to 10^4 Hz makes it very attractive for potential applications provided that its high dielectric losses can be minimized while keeping ε'_r as high as possible. In this context it is seen that samples with higher particle

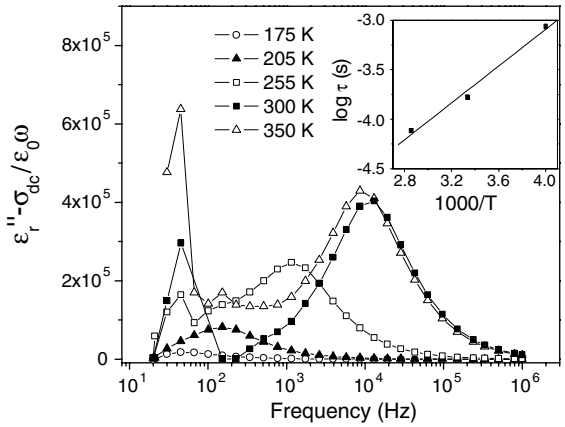

Figure 7. Frequency dependence of the imaginary part of the complex relative dielectric permittivity of the $CaMn_7O_{12}$ sample with $\phi \sim 1$ μm after subtraction of the contribution from free charge carriers (temperature range: 175 K $\leqslant T \leqslant$ 350 K). Inset: logarithm of the characteristic time (inverse of the characteristic frequencies) versus the inverse of temperature.

size are those exhibiting better dielectric properties. Even more, a very large static dielectric constant of the order of 10^7 is estimated for the case of a single crystal (infinite grain).

From the scientific point of view many questions should be answered about the origin of the observed dielectric behaviour and about its intrinsic or extrinsic nature.

With this aim, and as this material is not completely insulating, we have subtracted from the ε_r'' raw data the contribution from free charge carriers following equation (1):

$$\varepsilon''_{r,die}(\omega) = \varepsilon''_r(\omega) - \frac{\sigma_{dc}}{\varepsilon_0\omega}, \tag{1}$$

where $\varepsilon''_{r,die}$ is the dielectric contribution of the dielectric to ε_r'' and σ_{dc} is the dc electrical conductivity, which is obtained from the extrapolation of the conductivity, $\sigma(\omega)$, to low frequencies.

Figure 7 shows the results obtained for the $\phi = 1$ μm sample.

Very interestingly, when representing the so-obtained $\varepsilon''_{r,die}$ data as a function of frequency in addition to the maximum found at very low frequency—that is typical of diffusional processes—for $T > 250$ K a second maximum appears at $\sim 10^4$ Hz, the frequency at which the very high dielectric constant decreases in a step-like manner (figure 7). This second maximum resembles that of a Debye-like dipolar relaxation process with characteristic times, $\tau = 1/\omega$, where ω is the characteristic frequency of relaxation.

A logarithmic fit of the characteristic relaxation times versus the inverse of temperature (inset of figure 7) shows that these follow an Arrhenius type of behaviour, $\tau = \tau_0 \exp(U/k_B T)$, where U is the activation energy and k_B the Boltzmann constant. From this fit we have obtained $U \sim 185$ meV and $\tau_0 \sim 153$ ns for the case of the sample with $\phi = 1$ μm.

As for the reasons that would account for the appearance of electric dipoles in these samples, in principle they could have an extrinsic and/or intrinsic origin.

But the observed strong influence of the particle size and the nature of the contacts on their dielectric properties reveal that there is an important extrinsic contribution to the observed very high ε'_r values. In this context, the extrinsic interfacial Maxwell–Wagner model [23] allows us to explain the variations observed as the above factors are modified. In this context, for a typical Maxwell–Wagner two-layer condenser consisting of two parallel sheets of material (1) and (2), characterized by their dielectric constants, conductivities and thickness ($\varepsilon'_{r,1}$, σ_1, d_1)

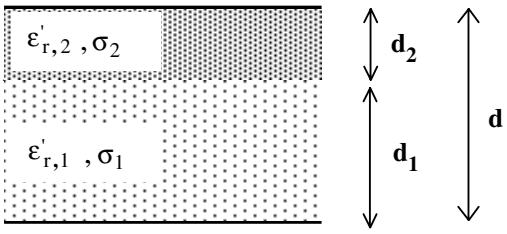

Figure 8. Model of a two-layer condenser consisting of two parallel sheets of material (1) and (2).

and ($\varepsilon'_{r,2}$, σ_2, d_2), respectively (figure 8), the optical dielectric constant, $\varepsilon'_{r,\infty}$, can be expressed as [24]

$$\varepsilon'_{r,\infty} = \frac{d\varepsilon'_{r,1}\varepsilon'_{r,2}}{\varepsilon'_{r,1}d_2 + \varepsilon'_{r,2}d_1} \tag{2}$$

with $d = d_1 + d_2$; and the dielectric constant at low frequencies (the so-called static dielectric constant, $\varepsilon'_{r,s}$) can be expressed as [24]

$$\varepsilon'_{r,s} = \varepsilon'_{r,\infty}\left\{1 + d_1 d_2 \left(\frac{\frac{1}{\sigma_1}\sqrt{\frac{\varepsilon'_{r,1}}{\varepsilon'_{r,2}}} - \frac{1}{\sigma_2}\sqrt{\frac{\varepsilon'_{r,2}}{\varepsilon'_{r,1}}}}{\frac{d_1}{\sigma_1} + \frac{d_2}{\sigma_2}}\right)^2\right\}. \tag{3}$$

If the subscript 1 represents the bulk material, that is its intrinsic behaviour, and the subscript 2 comprises factors such as electrode/sample interface and grain boundaries, that is extrinsic factors, and assuming that $\sigma_1 \gg \sigma_2$ and $d_1 \gg d_2$ and that $\varepsilon'_{r,1} \approx \varepsilon'_{r,2}$ we obtain, from equation (2),

$$\varepsilon'_{r,\infty} \approx \varepsilon'_{r,1}. \tag{4}$$

And from equation (3),

$$\varepsilon'_{r,s} \approx \varepsilon'_{r,1}\left\{1 + d_1 d_2 \left(\frac{\sigma}{d\sigma_2}\right)^2\right\}, \tag{5}$$

where σ is the static conductivity of the sample, which can be expressed as

$$\sigma = d\left(\frac{d_1}{\sigma_1} + \frac{d_2}{\sigma_2}\right)^{-1}. \tag{6}$$

According to expression (3), an increase in the surface layer, d_2, and a decrease in the sample conductivity gives rise, as seen in the experimental results, to a decrease of the static dielectric constant.

In addition, the observed particle size dependence of $\Delta\varepsilon'_r = \varepsilon'_s - \varepsilon'_\infty$ (figure 5) can also be explained on the basis of equation (5).

In this context, and following (5) we can express $\Delta\varepsilon'_r$ as

$$\Delta\varepsilon'_r = \varepsilon'_{r,s} - \varepsilon'_{r,\infty} \approx \varepsilon'_{r,\infty}\frac{d_2}{d_1}\left(\frac{\sigma}{\sigma_2}\right)^2. \tag{7}$$

If we take into account that the particle size dependence of these factors can be expressed as [25]

$$\frac{\sigma}{\sigma_2} \approx \sigma_0 e^{-A\frac{1}{\phi}} \qquad \text{and} \qquad \frac{d_2}{d} = B\frac{1}{\phi}, \tag{8}$$

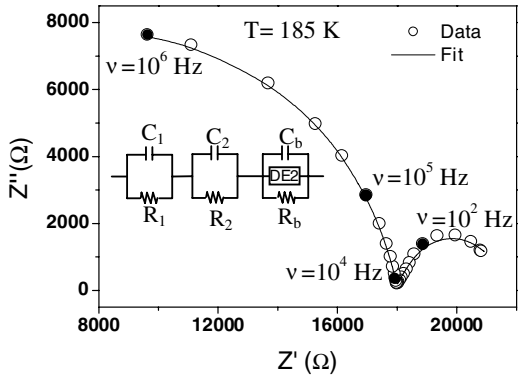

Figure 9. Impedance complex plane plot corresponding to the $CaMn_7O_{12}$ sample with particle size $\phi \sim 1\ \mu$m. The experimental data have been fitted on the basis of an equivalent circuit consisting of three parallel RC elements connected in series, one of them with a resistance that is frequency dependent.

where A and B are constants and ϕ is the particle size diameter, we arrive at the following expression for $\log \phi \approx$ constant and/or very small:

$$\log \Delta\varepsilon_r' \approx F - \frac{A}{\phi}, \tag{9}$$

where F is a constant. This equation (9) indicates that, when the above-mentioned conditions are fulfilled, there is a linear dependence of $\log \Delta\varepsilon_r'$ with the inverse of the particle size.

On the other hand, the variation of the ε_r' values upon contact substitution can also be understood on the basis of the above proposed model. Again, as predicted by the Maxwell–Wagner model in equation (5), as the conductivity of the sample increases when using sputtered gold contacts so does the dielectric constant.

Therefore extrinsic effects play an important role in the observed dielectric behaviour, especially at low frequencies and/or high temperatures.

One of the possible origins for such extrinsic effects is the formation of Schottky barriers at the contact–sample interface which, among other factors, depend on the area of direct metal–semiconductor contact. Different cluster sizes of the metals obtained during sputtering could account for the different dielectric constant values obtained when using silver and gold contacts (apart from other extrinsic factors such as size or thickness of the measured pellets).

In addition, grain boundary (internal) barrier layer capacitance (IBLC) arising from electrical heterogeneities in these polycrystalline samples could also be playing a role, as has been shown to occur in $CaCu_3Ti_4O_{12}$ samples [4].

In any case, to separate the contribution from the bulk (intrinsic) from extrinsic effects we have also performed complex plane analysis of the obtained data (see figure 9).

The best fits were obtained when modelling the impedance spectroscopy data on the basis of the equivalent circuit displayed in the inset of figure 9. It consists of two parallel RC elements connected in series, that would represent the contribution from interfacial polarization processes (electrode/sample and grain boundaries) (R_1C_1 and R_2C_2 in figure 9); meanwhile the bulk response is approximated by a capacitance C_b and a resistance R_b, that are frequency independent, and a frequency-dependent distributed element (DE). This DE, that is modelled as an impedance inversely proportional to a power of the frequency [21], is the typical signature of charge transport via hopping conductivity [26]. The fitted frequency exponent of this DE, that depends slightly on temperature, is around 0.7.

The fits using this equivalent circuit indicate that the capacitance of the intrinsic bulk response is of the order of magnitude of picofarads per centimetre while that of the interface capacitor is of the order of microfarads per centimetre. Also, the intrinsic dielectric constant calculated from the value of the obtained bulk capacitance, $\varepsilon'_{r,1} \approx \varepsilon'_{r,\infty}$, is of the order of 30. This $\varepsilon'_{r,\infty}$ is still rather high for this type of oxides [3, 24].

Having arrived at this point, it is interesting to think about the origin of such an enhanced intrinsic dielectric constant for this type of material. In this context it is interesting to note that in our research group we have also detected high dielectric constants in other oxides with charge ordering (CO) near their CO temperature, such as in $Pr_{0.67}Ca_{0.33}MnO_3$ [27] ($T_{CO} \approx 225$ K), where a fourfold increase of its dielectric constant is observed as the CO temperature of 225 K is crossed [28], or in $La_{1.5}Sr_{0.5}NiO_4$, where we have also found a pronounced increase at the CO temperature of 180 K [29]. In fact, these findings led us to search for materials that display a high dielectric constant at room temperature among systems that experience transitions to charge-ordered states at higher and more suitable temperatures. And apart from $CaMn_7O_{12}$ presented here, we have studied other compounds that also belong to this category, and we have found values of ε'_r of the same order of magnitude as the ones described here for $CaMn_7O_{12}$ in similar frequency and temperature ranges [30].

Also, in other systems where some members of the series show CO while others do not, we find much higher values in the case of the charge-ordered phases [31].

All these results lead us to associate this enhanced intrinsic dielectric constant to the fact that the charge separation that occurs in a CO transition could lead to the formation of some kind of electrical dipoles that form an electronic inhomogeneity in the system (leading to the observed relaxor dielectric behaviour) in an analogous way to that theoretically proposed by other authors very recently [32].

In addition to a high intrinsic dielectric constant, the extrinsic effects to which we referred before enhance even further the dielectric response of this material and give rise to such a very high room-temperature dielectric constant.

More work is in progress to optimize the dielectric behaviour of this material (by trying to minimize its dielectric losses while keeping ε'_r as high as possible) and also to completely clarify the origin of its enhanced intrinsic dielectric constant.

5. Conclusions

We have studied the dielectric properties of the $CaMn_7O_{12}$ compound, finding a very high dielectric constant value at room temperature that could be very attractive for practical applications provided that the associated dielectric losses can be lowered.

This high dielectric constant is strongly enhanced by extrinsic polarizations effects.

An intrinsic dielectric constant of 30 is estimated, and this value is already relatively high for such type of compounds.

We relate the enhanced intrinsic dielectric constant of this mixed oxide to the presence of the electronic process of charge ordering in this material.

Acknowledgments

The authors are grateful for financial support from MEC (Spain) and UE (FEDER) under project MAT 2004-05130 and B Rivas-Murias and S Yáñez-Vilar want to thank MEC of Spain for their FPI fellowships.

References

[1] Haertling G H 1999 *J. Am. Ceram. Soc.* **82** 797
[2] Homes C C, Vogt T, Shapiro M, Wakimoto S and Ramírez A P 2001 *Science* **293** 673

[3] Lunkenheimer P, Bobnar V, Pronin A V, Ritus A I, Volkov A and Loidl A 2002 *Phys. Rev.* B **66** 052105
[4] Sinclair D S, Adams T B, Morrison F D and West A R 2002 *Appl. Phys. Lett.* **80** 2153
[5] Cohen M H, Neaton J B, He L and Vanderbilt D 2003 *J. Appl. Phys.* **94** 3299
[6] Lunkenheimer P, Fitchl R, Ebbinghaus S G and Loidl A 2004 *Phys. Rev.* B **70** 172102
[7] Cava R J, Fleming R M, Littlewood P, Rietman E A, Schneemeyer L F and Dunn R G 1984 *Phys. Rev.* B **30** 3228
[8] Littlewood P 1987 *Phys. Rev.* B **36** 3108
[9] Herzfeld K A 1927 *Phys. Rev.* **29** 701
[10] Portengen T, Östreich Th and Sham L J 1996 *Phys. Rev.* B **54** 17452
[11] Verwey E J W 1939 *Nature* **144** 327
[12] Kuwahara H and Tokura Y 1998 *Colossal Magnetoresistance: Charge Ordering and Related Properties of Manganese Oxides* ed C N R Rao and B Raveau (Singapore: World Scientific)
[13] Troyanchuk I O and Chobot A N 1997 *Crystallogr. Rep.* **42** 983
[14] Bochu B, Buevoz J L, Chenavas J, Collomb A, Joubert J C and Marezio M 1980 *Solid State Commun.* **36** 133
[15] Przenioslo R, Sosnowska I, Hohlwein D, Hauß T and Troyanchuk I O 1999 *Solid State Commun.* **111** 687
[16] Licci F, Besagni T and Rinaldi L 1985 *European Patent Specification* 85860253-2
[17] Howard C J, Hunter H and Rietica B A 2000 *A Computer Program for Rietveld Analysis of Organization* Lucas Heights Research Laboratories
[18] Lunkenheimer P, Rudolf T, Hemberger A, Pimenov S, Tachos S, Lichtenberg F and Loidl A 2003 *Phys. Rev.* B **68** 245108
[19] Lixin H, Neaton J B, Cohen M H, Vanderbilt D and Homes C C 2002 *Phys. Rev.* B **65** 214112
[20] Viana R, Lunkenheimer P, Hemberger J, Böhmer R and Loidl A 1994 *Phys. Rev.* B **50** 601
[21] Ross Macdonald J 2003 *LEVM version 8.0 Complex Nonlinear Squares Fitting Program*
[22] Przenioslo R, Sosnowska I, Suard E, Hewat A and Fitch A N 2002 *J. Phys.: Condens. Matter* **14** 5747
[23] Maxwell J C 1982 *Electricity and Magnetism* (Oxford: Clarendon)
[24] Von Hippel A 1995 *Dielectrics and Waves* (Boston, MA: Artech House Publishers)
[25] Glittleman J I, Goldstein Y and Bozowski S 1972 *Phys. Rev.* B **5** 3609
[26] Elliot S R 1987 *Adv. Phys.* **36** 135
[27] Rivadulla F, López Quintela M A, Hueso L E, Jardón C, Fondado A, Rivas J, Causa M T and Sánchez R D 1999 *Solid State Commun.* **110** 179
[28] Jardón C, Rivadulla F, Hueso L E, Fondado A, Rivas J, López Quintela M A, Zysler R, Causa M T and Sande P 1999 *J. Magn. Magn. Mater.* **196/197** 475
[29] Rivas J, Rivas-Murias B, Fondado A, Mira J and Señarís-Rodríguez M A 2004 *Appl. Phys. Lett.* **85** 6224
[30] Yáñez-Vilar S, Castro-Couceiro A, Rivas-Murias B, Fondado A, Mira J, Rivas J and Señarís-Rodríguez M A 2005 *ZAAC* **631/11** 2265
[31] Castro-Couceiro A, Sánchez-Andújar M, Rivas-Murias B, Mira J, Rivas J and Señarís-Rodríguez M A 2005 *Solid State Sci.* **7** 905
[32] Efremov D V, Brink J and Khomskii D I 2004 *Nat. Mater.* **3** 853